Assessment of offshore wind conditions in coastal areas of Japan using single scanning Doppler LiDAR

A Mano[1], A Ueno[1], S Itozaki[1], T Ishihara[2]

[1] RENOVA, Inc., 2-2-1 Kyobashi, Chuo-ku, Tokyo 104-0031, Japan
[2] The University of Tokyo, 7-3-1 Hongo, Bunkyo-ku, Tokyo 113-8656, Japan

a_mano@renovainc.com, ishihara@bridge.t.u-tokyo.ac.jp

Abstract. In this study, offshore wind conditions in coastal areas of Japan measured by single scanning Doppler lidar is investigated. The effects of measurement range as well as rainfall and snowfall on data availability of the Doppler scanning lidar are examined. Data filtering criteria are then proposed and verified by data thinning to meet both accuracy and post-processed data availability requirements for offshore wind measurements at multiple altitudes. Finally, one-year offshore wind measurement with three different elevation angles is conducted using a single Doppler scanning lidar to investigate wind conditions in the coastal region of Northern Japan. It is found that the accuracy of 15-second average wind speed measurements by PPI (Plan Position Indicator) scan depends on the sector size. An accurate 10-minute mean wind is measured when the sector size is larger than 39 degrees and proportion of valid data acquisition is more than 10% of the time duration. The vertical and horizontal distributions of offshore wind speed in different wind directions are also analyzed and the effects of onshore topography on offshore wind conditions are clarified.

1. Introduction

In recent years, expectations for offshore wind power have been increasing in Japan. Accurate measurements of wind speed are essential for assessment of site suitability and annual energy production. The use of offshore met masts is the most reliable method measuring offshore wind conditions but is cost prohibitive. As such, floating lidar is used in many offshore projects. Use of floating lidar can allow for reliable mean wind speed calculations, but they are still unable to provide reliable measurements of turbulence characteristics, including turbulence intensity [1, 2, 3, 4]. Another risk with the use of floating lidar is that the mooring lines can break under severe weather conditions and the buoy can become adrift. To overcome these problems, land-based scanning lidars have been used for offshore wind measurements [5, 6, 7, 8 ,9]. Although the measurement range is limited to a few kilometers from the coastline, land-based scanning lidar is considered one of the solutions for nearshore projects in Japan.

Scanning lidar measurement can be divided into three categories according to the number of scanning lidar used: one scanning lidar (hereafter referred to as "single scanning lidar"); two scanning lidars (hereafter referred to as "dual scanning lidar"); and three scanning lidars (hereafter referred to as “triple scanning lidar”). In a typical single scanning lidar measurement, line of sight (LoS) velocity is measured during a PPI scan [10] for a fixed sector width centred to the direction of the observation point, and horizontal wind velocity is estimated assuming homogeneity of the wind field in time and space during a scan. The advantage of single scanning lidar measurement is the expectation of higher data availability because only one lidar is used for the measurement. On the other hand, in dual lidar measurement, two lidars have a fixed azimuth angle to the direction of the measurement target and LoS velocity is measured.

The horizontal wind speed can be estimated only by assuming that mean vertical wind speed is zero. With dual scanning lidar it is not necessary to assume the homogeneity of the wind field and is widely used to measure mean wind speed and direction as well as turbulence in Japan. Watanabe et al. [5] used dual scanning lidar with elevation angles of 0.77 and 0.84 degrees and a range resolution of 50 m to measure wind conditions at a met mast 3 km away and showed that the estimated turbulence intensities were in good agreement with those obtained from the met mast's cup anemometers. However, the cost is twice as much as single scanning lidar, and the system availability and the post-processed data availability are lower than those of single scanning lidar [6]. Triple scanning lidar directly measures the three wind speed components, therefore the assumption that mean vertical wind speed is zero is not required and turbulence characteristics is allowed to be measured. However, data availability is even lower than with dual scanning lidar [8]. For multiple lidar strategy, the measured wind speed is averaged over a large area. Cheynet et al. [9] used a triple scanning lidar strategy based on WindCube 200S to measure the turbulence intensity above the surface of the sea in Norway. The flow was measured 4 - 4.5 km away using lidars with a range resolution of 75 m. The intersection of the beams at an angle of almost 90 degrees meant that the flow was studied within a large surface such as a disc with a radius of 75 m, leading to an underestimation of the turbulence intensity due to the spatial averaging effect.

In lidar measurements, careful consideration of the observation distance is crucial. This is due to the decrease in data availability as the distance from the target increases. Previous studies, such as a study by Carbon Trust and RES [11], have reported on data availability and measurement range but have not considered the impact of rain and snow, which are prevalent in the Japanese climate and significantly affect data quality. Moreover, using single scanning lidar measurements implies a reliance on sector scanning. Although the reconstruction method was proposed by Simon and Courtney [12], it does not adequately discuss data availability issues. Since accuracy and post-processed data availability are trade-offs, it is necessary to establish criteria that balance accuracy and post-processed data availability.

In addition, few studies include the sufficient one-year measurement period needed to comprehensively analyze data availability. There has been research into vertical profiles in nearshore, but the data availability was low [8]. European offshore wind farms are typically located tens of kilometres from the coast, while Japanese offshore wind farms are planned closer to shore, only a few kilometers away. This proximity necessitates an accurate assessment of the wind measurement in relation to the influence of the nearby onshore topography.

This study focuses on validation and offshore wind observation with single scanning lidar measurements. Firstly, the variation of data availability with measurement range, rainfall and snowfall is investigated, and the criteria that meet the requirements of both data availability and measurement accuracy for the reconstruction of the horizontal wind speed and for the 10-minute mean wind speed are investigated. The accuracy of the single scanning lidar measurement is then validated by comparison with the met mast measurement near the coast. Secondly, one year of offshore wind measurements at two sites are carried out using single scanning lidar measurements at three different heights and system availability and post-processed data availability with the proposed methods are examined. The vertical shear and horizontal distributions of offshore wind speed in each wind direction are also analyzed and the effects of onshore topography on the offshore wind conditions are discussed.

2. Method and instrumentation

The overview of single scanning lidar measurement is described in section 2.1. The site and lidar settings are described in section 2.2.

2.1. Overview of single scanning lidar measurement

In this study, to measure wind conditions with single scanning lidar, the PPI mode measurement is performed. Figure 1 (a) shows relationship between LoS wind speed and the horizontal and vertical components of wind speed with PPI mode measurement.

Assuming that wind conditions are uniform over the spatial extent and duration of one scan, the spatio-temporally averaged wind speed and direction for each one scan can be reconstructed from the LoS velocity u_r using the methods proposed by Simon and Courtney [12]. The averaged velocity components $\overline{u}$ and $\overline{v}$ are calculated by the least-squares method using equations (1) and (2) as follows,

$$\overline{u} = \frac{\sum_{i=1}^{i=n}(\hat{u}_{ri} * \cos\ \theta_i) * \sum_{i=1}^{i=n}(\sin^2\ \theta_i) - \sum_{i=1}^{i=n}(\hat{u}_{ri} * \sin\ \theta_i) * \sum_{i=1}^{i=n}(\cos\ \theta_i * \sin\ \theta_i)}{\sum_{i=1}^{i=n}\cos^2\ \theta_i * \sum_{i=1}^{i=n}\sin^2\ \theta_i - (\sum_{i=1}^{i=n}(\cos\ \theta_i * \sin\ \theta_i))^2} \quad (1)$$

$$\overline{v} = \frac{\sum_{i=1}^{i=n}(\hat{u}_{ri} * \sin\ \theta_i) * \sum_{i=1}^{i=n}(\cos^2\ \theta_i) - \sum_{i=1}^{i=n}(\hat{u}_{ri} * \cos\ \theta_i) * \sum_{i=1}^{i=n}(\cos\ \theta_i * \sin\ \theta_i)}{\sum_{i=1}^{i=n}\cos^2\ \theta_i * \sum_{i=1}^{i=n}\sin^2\ \theta_i - (\sum_{i=1}^{i=n}(\cos\ \theta_i * \sin\ \theta_i))^2} \quad (2)$$

where θ_i is the azimuth angle of each LoS velocity u_{ri}. $\hat{u}_{ri}$ is equal to $u_{ri}/\cos\varphi$ and φ is the elevation angle. The subscript i is the number of the LoS velocity and n is 15 in this study. The mean wind speed and direction for one scan is calculated by vector composition and inverse trigonometric function from $\overline{u}$ and $\overline{v}$ as shown in equations (1) and (2).

The PPI mode is used with a sector size of 45 degrees and a scan speed of 3 degrees/s is adopted to obtain 15 LoS velocities in one scan. The angle covered by valid data is defined as the sector size in this study. Figure 1 (b) illustrates the definition of the sector size. In this example, the left and right edges of the valid data from the lidar correspond to the 3rd and 11th positions from the left, respectively, resulting in a sector size of 27 degrees. This sector size does not depend on the number of valid data points. To investigate the effects of sector size and number of valid data points in 15-second average on the measurement accuracy, the data acquisition rate η_x is defined as shown in equation (3).

$$\eta_x = \frac{Number\ of\ valid\ data\ points}{Total\ number\ of\ data\ points} \times 100 \quad (3)$$

The 15-second average velocity components are used to obtain the 10-minute mean wind speed. The effect of sector size on measurement accuracy is investigated on 15-second average wind speed. The relationship between the accuracy and η_x is discussed in section 3.1.

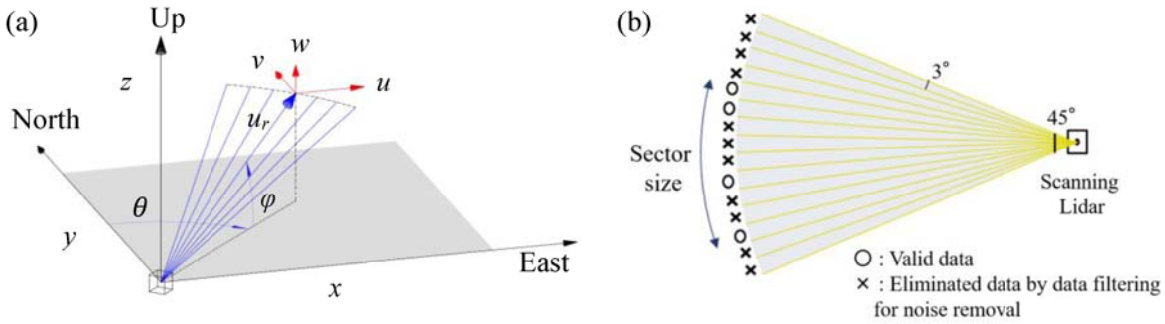

Figure 1. (a) Relationship between line-of-sight (LoS) wind speed and horizontal and vertical velocity components of wind speed, (b)Definition of sector size

Figure 2 (a) shows a schematic diagram of the single scanning lidar measurements for the offshore wind. A lidar performs offshore wind measurements at three different heights using three scans A, B, and C. Figure 2 (b) shows the order of these three scans A, B and C, the scan period, and the scan head movement time for changing the laser LoS. Since three heights are observed, the number of 15-second averages included in the 10-minute mean is approximately one-third that of observing only one height. However, as shown in section 3.1, if 4 or more valid 15-second averages are obtained over a 10-minute period, the proposed criteria are met and accuracy is guaranteed. As shown in Figure 2 (b), the timestamp of the 15-second average defines the data to be included in a 10-minute mean. The three data filters used in this study as explained in section 3.1 are listed below.

(1) Use data with manufacturer recommended status 1 for noise removal.
(2) Obtain the 15-second average velocity components from the LoS velocity of the scanning lidar and include at least three valid data points with a sector size of 39 degrees or more.
(3) Calculate the 10-minute mean wind speed and direction, including four or more valid 15-second average values.

Eight days of observational data are used to verify the accuracy and stationarity of the proposed scanning. The 10-minute means for 1/3 of the observation time are compared to those for the entire time. For wind speed, the slope is 1.00 and the coefficient of determination is 1.00; for wind direction, the slope is 1.00, the offset is -0.72 and the coefficient of determination is 0.99.

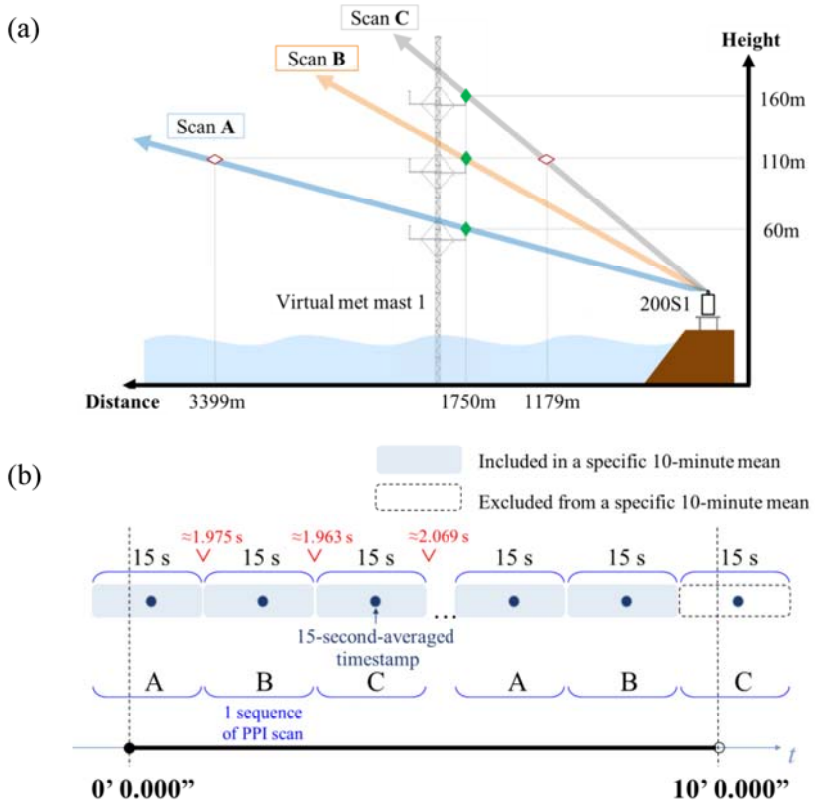

Figure 2. Schematic diagram of (a) single scanning lidar measurements at three heights and (b) procedure of measurements for scans A, B and C

2.2. Description of sites and lidar settings

Two Vaisala WindCube 200S lidars are used in this study. Hereafter, each instrument will be referred to as 200S1 and 200S2, respectively, as shown in Figure 3. 200S1 is installed in the Michikawa area. The landward side has hills rising 100 - 200 m above the surrounding land. 200S2 is installed in the Honjo area and is near the mouth of the Koyoshi River, which flows toward the SSE direction. The landward side has a flat urban area. 200S2 is also used to validate the proposed filtering criteria described in section 3.1.

Offshore wind measurements at three different heights are performed. The offshore measurement targets called virtual met masts are located at a distance of 1750 m from 200S1 and a distance of 1309 m from 200S2, respectively, as shown in Figure 3 (a) and (b). The hub height is set to 110 m in this study. The scan settings, measurement height and measurement period are shown in Table 1 (a) and (b). The minimum gate range length for the WindCube 200S is 25 m. A short gate range length provides better accuracy due to a smaller averaging area, but a larger averaging area provides a higher data acquisition rate. In this study, data availability is prioritized and gate range lengths of 50m and 100m are adopted since offshore winds are nearly uniform.

To validate the accuracy of single scanning lidar measurement, the PPI mode measurement is performed in the direction of the met mast, and the wind speed and wind direction are compared with those from a cup anemometer and a wind vane mounted on the met mast. Figure 3 (c) shows the locations

of the scanning lidar and the met mast. The target point is located at a horizontal distance of 1340 m and a height of 57.5 m. Table 1 (c) summarises the scan settings. One scan obtains 15 LoS velocities in 15 seconds. Each LoS velocity is presented by red dots in the measurement area as shown in Figure 3 (c). Note that the wind conditions within the scan area are assumed to be uniform over the spatial extent, but the scan area includes both offshore and onshore areas and the wind speed distribution may not be uniform depending on the wind direction. The influence of this on single scanning lidar measurement accuracy validation is discussed in section 3.1

The single scanning lidars are mounted on rigid bases which consisted of steel plates and frames on concrete foundations to ensure pointing accuracy. The elevation and azimuth angles of the lidar have errors due to changes in the optical path caused by backlash in the gears of the instrument's scanning head and assembly tolerances of the optical components. The offset values are applied to minimize the error over the scan area by surveying at least three hard targets and determining error functions for azimuth and elevation angles. In this study, a sinusoidal curve is used as the error function, and the maximum error is less than 0.11 degrees in azimuth and 0.03 degrees in elevation. This means that the errors at the target point are less than 3 m in the horizontal direction and 1 m in the vertical direction. These errors are very small compared to the target point height and the arc area scanned in the PPI mode.

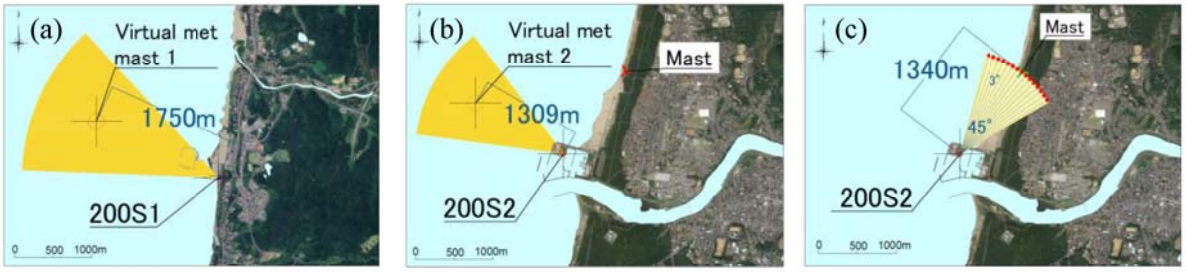

Figure 3. Locations and PPI scan area of lidars. (a) 200S1, (b) 200S2, (c) 200S2 when performing validation with a met mast.

Table 1. Description of scan setting of scanning lidars and measurement period

	(a) Offshore observation	(b) Offshore observation	(c) Validation with met mast
Measurement equipment	200S1	200S2	200S2
Scan mode	PPI	PPI	PPI
Scan sector size	45 deg.	45 deg.	45 deg.
Range resolution	100 m	100 m	50m,100m
Accumulation time	1 s	1 s	1 s
Scan speed	3 deg./s	3 deg./s	3 deg./s
Azimuth angle	294.2 deg.	299.7 deg.	36.8 deg.
Measurement heights for three Scans A, B, C (Elevation angles)	Scan A: 60 m (1.8 deg.) Scan B: 110 m (3.4 deg.) Scan C: 160 m (5.0 deg.)	Scan A: 62 m (2.5 deg.) Scan B: 110 m (4.6 deg.) Scan C: 158 m (6.7 deg.)	57.5 m (2.5 deg.)
Measurement period	1 year	1 year	39 days

3. Results and discussion

Accuracy of single scanning lidar measurement is validated in section 3.1. The variation of data availability with measurement range, rainfall and snowfall is investigated. The criteria of data filtering are examined to meet the requirements of both accurate measurement of mean wind speed and high data availability. Criteria for determining appropriate valid data that satisfies both measurement accuracy and post-processed data availability are presented, and the accuracy of single scanning lidar measurement is validated using the met mast.

The offshore wind measurements by single scanning lidars are then described in section 3.2. System availability and post-processed data availability of the scanning lidars based on the method proposed in this study are evaluated using one year of offshore wind measurement data at two sites with different

onshore topography. An overview of the offshore wind measurements is described, and the vertical profiles and horizontal distributions of wind speeds in each sector are examined to clarify the effects of onshore topography on the nearshore wind conditions.

3.1. Validation of single scanning lidar measurement

The scanning lidar measures LoS velocity from the Doppler shift by emitting a laser of a specific frequency into space and receiving the reflected light from aerosols in the atmosphere. It is directly affected by weather conditions, with rain and snow reducing the quality of the measurement data. The relationship between data availability and measurement range is investigated. Here, data availability is defined as the ratio of the number of measurements after data filtering to the number of all measurements. CNR (carrier-to-noise ratio), Mean Error (average error between the received Doppler spectrum and the spectrum reconstructed by instrument processing), and $\sigma_{V\gamma}$ (variance reflecting wind speed fluctuations during the measurement) are used as data filters. The CNR threshold applied is -29 dB.

The range of measured azimuth angles is approximately 270 to 320 degrees, indicating that the laser is aimed at an unobstructed ocean. The elevation angles are set to 2 degrees. This means that the measurement range of 500 - 8500 m corresponds to a height of 17.4 - 296.6 m, and the measurement range even at 8500 m is set to not reach 500 m in height in order to eliminate the impact of differences in aerosol concentration on the data availability. The velocity of falling rain is typically around 6.5 m/s and is estimated to increase LoS velocity by 0.57 m/s at the elevation angle of 5 degrees as indicted in the Offshore Wind Measurement Guidebook [13]. This effect is not considered in this study because no rain gauges are installed at the offshore observation sites. Since the average percentage of rainy days in this area in the past 30 years is 24%, and the actual duration of rain is shorter than this percentage, the effect of rain on the LoS velocity is estimated to be less than 0.14 m/s. The measurement period was 3600 hours, and rainfall and snowfall hours reported by the nearby AMeDAS were 1345 and 35 hours, respectively.

Figure 4 shows the variation of data availability with measurement range for all data including rain and snow conditions. Data availability decreases as the measurement range increases. The measurement range where data availability exceeds 80% is within 4.5 km for all data, within 2 km when rainfall is less than 10 mm/h, and within 5 km when snowfall is less than 1cm/h. In this region, a measurable range of 2 km or less must be considered in order to achieve sufficiently high data availability.

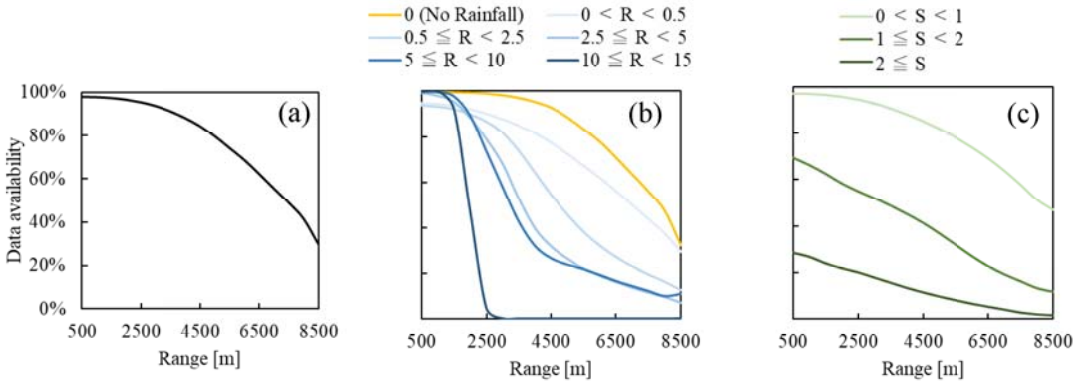

Figure 4. Variation of data availability with measurement range and precipitation (a) with all data including rain and snow, (b) with different amount of rainfall and (c) snowfall. The units of legend for rainfall (R) and snowfall (S) are mm/h and cm/h, respectively.

To improve measurement accuracy, low quality data must be excluded. However, stricter exclusion criteria will reduce the post-processed data availability. Therefore, it is necessary to find a criterion that meets the requirements of both measurement accuracy and post-processed data availability.

Here, criteria are considered for the 15-second averages as a first step and for the 10-minute mean as a second step. The post-processed data availability when applying the proposed criteria is then examined using six months of offshore measurement data.

The data acquisition rates for η_{20}, η_{40}, and η_{60} are generated by randomly thinning the 15 valid LoS velocities obtained from actual measurement data. Figure 5 (a) and (b) show the variation of coefficient of determination R^2 and slope with sector sizes for η_{20}, η_{40}, and η_{60}. The figures in parentheses represent the number of valid data points. Even in the case of η_{20}, highly accurate R^2 and slope can be obtained when the sector size is large. This indicates that measurement accuracy is highly dependent on the sector size. Here, accuracy is discussed with reference to KPI and acceptance criteria proposed by Carbon Trust [14]. For sector sizes larger than or equal to 39 degrees, R^2 is larger than or equal to 0.97 and slope is between 0.97 and 1.03, meeting the minimum acceptance criteria. Therefore, it is proposed that the number of valid data points for the 15-second average to be 3 or more, and a sector size of 39 degrees or more as criteria of data filtering.

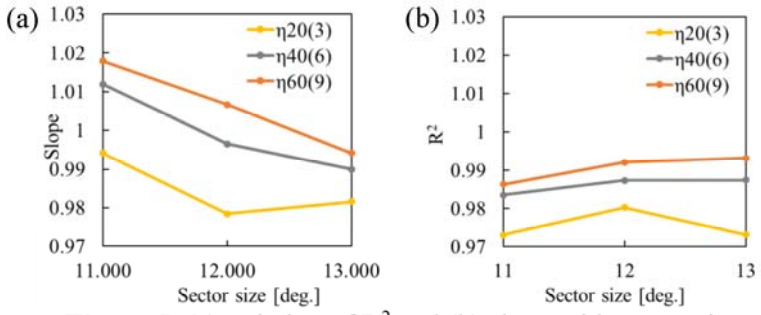

Figure 5. (a)variation of R^2 and (b) slope with sector size

The impact of the proposed criteria on the post-processed data availability is investigated using six months of offshore wind measurement data from winter to early summer. The frequencies of sector sizes of 9 - 36 degrees, 39 - 42 degrees, and 45 degrees are 0.8%, 0.6%, and 98.6%, respectively. Sector sizes less than 39 degrees occur 0.8% of the time, so excluding them has a small impact on the post-processed data availability.

The effect of the number of valid 15-second average data points on the accuracy of the 10-minute mean wind speed is also examined and the data acquisition rate η_x as shown in equation (3) is employed again. The number of 10-minute mean wind speed datasets is 465. The 10-minute mean wind speed is obtained from the two 15-second average velocity components. Table 2 shows the R^2 of the 10-minute mean wind speed at data acquisition rates $\eta_{2.5}$ to η_{80}. The correlation decreases as the data acquisition rate decreases. In this study, η_{10} is selected as the criterion, which refers to the best practice of the acceptance criteria proposed by the Carbon Trust [14]. The total amount of data in equation (3) is 34 to 36 depending on the timing, so when η_{10} or more, the number of valid 15-second average data points is 4 or more. In this study, the criterion for determining the number of valid data points for the 10-minute mean is 4 or more valid 15-second averages, representing a minimum of 10% of the time duration of the 10 minutes.

Table 2. R^2 of 10-minute mean wind speed for $\eta_{2.5}$ ~η_{80}

	$\eta_{2.5}$	η_5	η_{10}	η_{20}	η_{40}	η_{60}	η_{80}
R^2	0.959	0.979	0.989	0.995	0.995	0.999	1.000

The accuracy of single scanning lidar measurement is validated using the met mast. The measurement settings and locations are shown in Figure 3 (c) and Table 1 (c). As mentioned in section 2.2, the wind conditions within the scan area are assumed to be uniform over the spatial extent, but the scan area includes both offshore and onshore areas as shown in Figure 3 (c), and the wind speed distribution may not be uniform depending on the wind direction. To discuss this issue, a three-dimensional flow analysis to predict the wind field is performed using a CFD software, MASCOT [15], and it was considered that

the flow is affected by wind direction over the scan area. Only the wind directions that guarantee uniformity of wind speed are subject to validation. Therefore, only data with wind direction in the range of 50 - 125 degrees and 260 - 320 degrees are used for accuracy evaluation [16]. Since wind speed and direction fluctuate significantly at low wind speeds, wind speed data below 2 m/s are excluded in this study. Figure 6 shows a comparison of the 10-minute mean wind speed and direction measured by the single scanning lidar measurements and the met mast. The slope and R^2 of wind speed are 1.02 and 0.98, respectively, and the slope, offset and R^2 of wind direction are 1.01, 1 and 0.99, respectively, which correspond to the best practice proposed by the Carbon Trust [14].

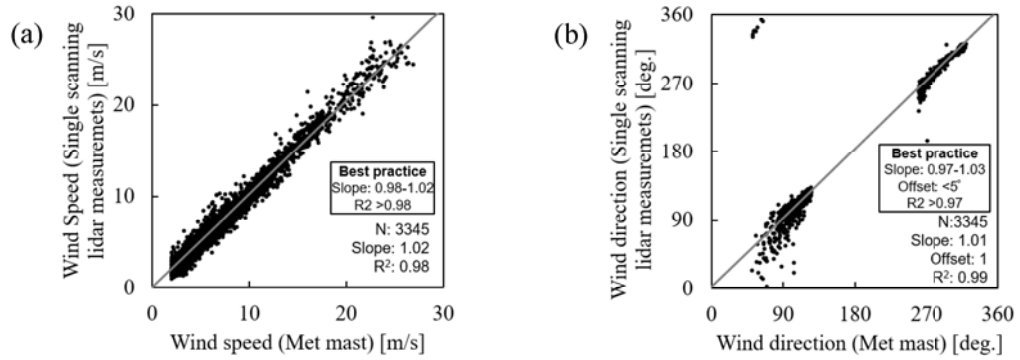

Figure 6. Comparison between wind speed and wind direction reconstructed by the single scanning lidar measurements and ones measured by a met mast at a height of 57.5 m. (a) Wind speed (b) Wind direction.

3.2. Offshore wind measurements by single scanning lidars

The offshore wind measurements by single scanning lidar are performed using the proposed criterion for data filtering as described in section 2.1. The scan settings and locations are described in section 2.2, Figure 3 (a) and (b), and Table 1 (a) and (b). Table 3 shows the system availability (SA) and the post-processed data availability (PDA) for the single scanning lidars during one year of measurements. The overall data availabilities of 10-minute mean wind speeds obtained from 200S1 at the heights of 60 m, 110 m, and 160 m are 96.5%, 96.3%, and 96.0%, respectively, and those from 200S2 at 62 m, 110 m, and 158 m are 97.7%, 97.6%, and 97.4%, respectively. The PDA is slightly lower at higher measurement heights due to the longer observation distance. For 200S1, the monthly SA is lower in the 10th month, but this is due to interruption in power supply to the lidar by a lightning strike. Except for this month, both 200S1 and 200S2 meet the Stage 3 requirements for one-year observation proposed by the Carbon Trust [14]. This indicates that the criteria proposed in this study satisfy both requirements for measurement accuracy and post-processed data availability.

Table 3. Summary of SA and PDA of single scanning lidar measurements for 200S1 and 200S2

	200S1				200S2			
		PDA [%]				PDA [%]		
	SA [%]	60m	110m	160m	SA [%]	62m	110m	158m
Month 1	100.0	96.9	97.1	96.7	100.0	97.0	97.4	97.0
Month 2	99.9	97.5	97.4	97.4	98.0	95.5	95.3	95.3
Month 3	100.0	89.0	88.9	88.6	100.0	89.8	89.8	89.7
Month 4	100.0	98.0	98.1	98.0	99.0	96.6	96.8	96.8
Month 5	100.0	99.4	99.1	98.8	100.0	99.3	99.3	99.3
Month 6	100.0	99.4	98.2	97.1	100.0	99.5	98.3	97.5
Month 7	96.4	95.1	94.5	94.0	96.8	96.7	96.4	95.9
Month 8	100.0	97.0	96.8	96.3	100.0	99.6	99.6	99.5
Month 9	100.0	99.5	99.5	99.3	100.0	99.9	99.9	99.9
Month 10	89.4	87.7	87.7	87.6	100.0	99.8	99.6	99.2
Month 11	99.1	98.3	98.3	98.4	99.1	98.8	98.8	98.9
Month 12	100.0	99.8	99.7	99.7	100.0	99.6	99.7	99.7
Overall	98.8	96.5	96.3	96.0	99.4	97.7	97.6	97.4

Figure 7 shows the seasonal variation in frequency of wind direction occurrence at the hub height of 110m in each wind direction obtained from two single scanning lidars of 200S1 and 200S2. The prevailing wind directions vary depending on the season. Sea winds are mainly observed from the northwest (NW) and west-northwest (WNW) in winter and spring as shown in Figure 7 (d) and (a), while land winds from the east-southeast (ESE) are more frequent in summer and autumn and less frequent in winter and spring. The prevailing winds from the southeast (SW) are only observed at the beginning of summer as shown in Figure 7 (b). It is found that the frequency of wind speed occurrence at the two sites is very similar.

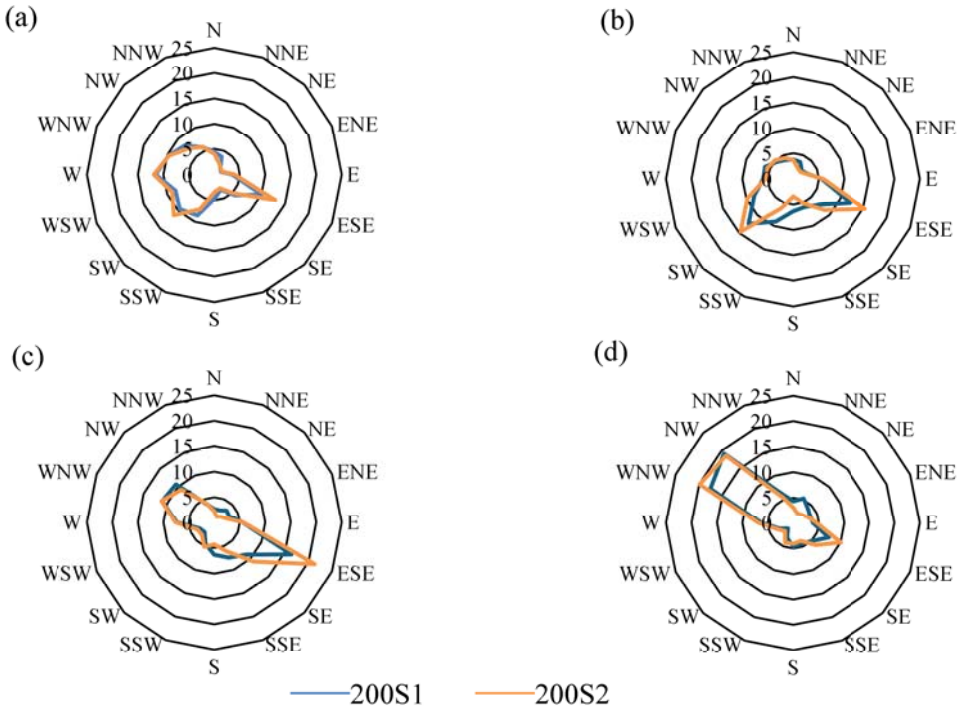

Figure 7. Seasonal variation in frequency of occurrence. (a) March to May, (b) June to August, (c) September to November, and (d) December to February corresponding to spring, summer, autumn and winter.

Figure 8 shows the comparison of vertical profiles of mean wind speed obtained for two single scanning lidars of 200S1 and 200S2 at each virtual met mast location. The wind speeds are normalized by the wind speed measured at the hub height of 110 m in each wind direction, The empirical power law profile with exponent α of 0.1 in open sea [17] is also shown in Figure 8.

The vertical profiles of 200S1 and 200S2 are similar in the sea winds from the south-southwest (SSW) to north-northwest (NNW). while the significant differences between them are observed in the land winds from southeast (SE) to south (S) due to the nearby topography. The negative shears are observed from southeast (SE) to south (S) at 200S2 only as shown in Figure 8 (g), (h) and (i). As shown in Figure 1(b), the Koyoshi River in the south-east direction is near 200S2. River winds are thought to generate low-level jets. As shown in Figures 8 (o) and (k), both north-westerly and south-westerly winds blow from offshore, but their exponents are different. When the wind is blowing from the northwest (NW), the exponent is close to zero, but when the wind is blowing from the southwest (SW), the exponent is large. This is due to differences in atmospheric stability depending on the season. As shown in Figure 7, the wind mainly blows from the northwest (NW) in winter and from the southwest (SW) in summer. In winter, the sea surface temperature in northern Japan is higher than the air temperature. Atmospheric stability is unstable, which promotes vertical mixing of air and reduces wind shear. In summer, the relationship between the sea surface and air temperatures is reversed, vertical mixing of air flow is suppressed, and large wind shear occurs.

Figure 9 shows a comparison of vertical profiles of wind direction difference at each virtual met mast location. The wind direction difference is calculated by subtracting the wind direction measured at the hub height of 110 m for each wind direction. Regarding the vertical profiles of wind direction, the trends are almost the same for all wind directions because 200S1 and 200S2 are in the same coastal area and there are no significant differences in meteorological conditions.

One single scanning lidar can simultaneously measure wind speeds at multiple points on the LoS, making it possible to observe wind speeds from approximately 200 m to several kilometers from the coast at once. Therefore, it is possible to observe wind speeds at multiple points in the horizontal direction as shown in Figure 2 (a). In this study, the wind speeds at the hub height of 110 m are extracted from scans A, B, and C. The horizontal distances from the single scanning lidar 200S1 to the observation points are 1179 m, 1750 m, and 3399 m, and those from 200S2 are 898 m, 1309 m, and 2408 m, respectively.

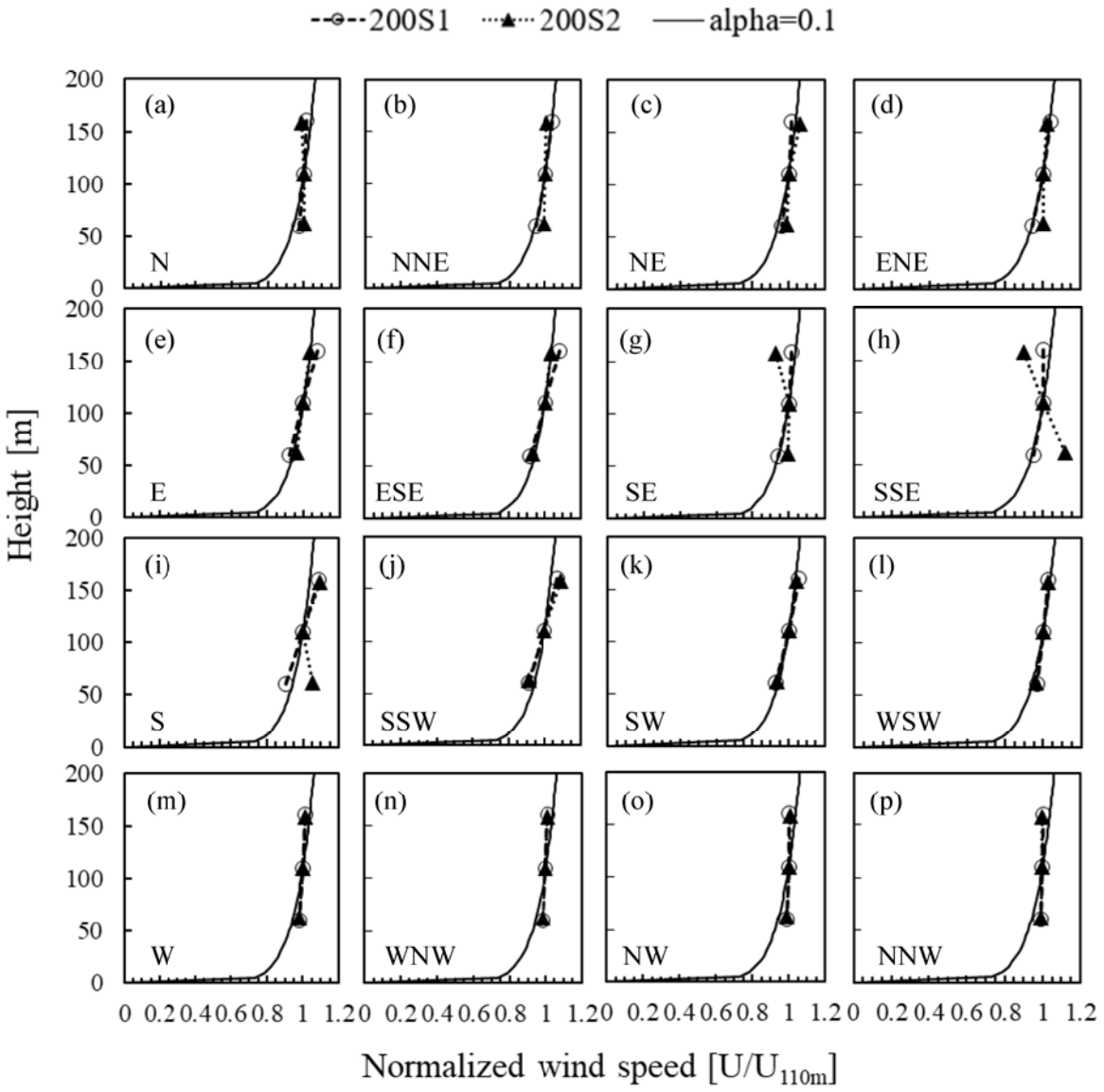

Figure 8. Vertical profiles of wind speed

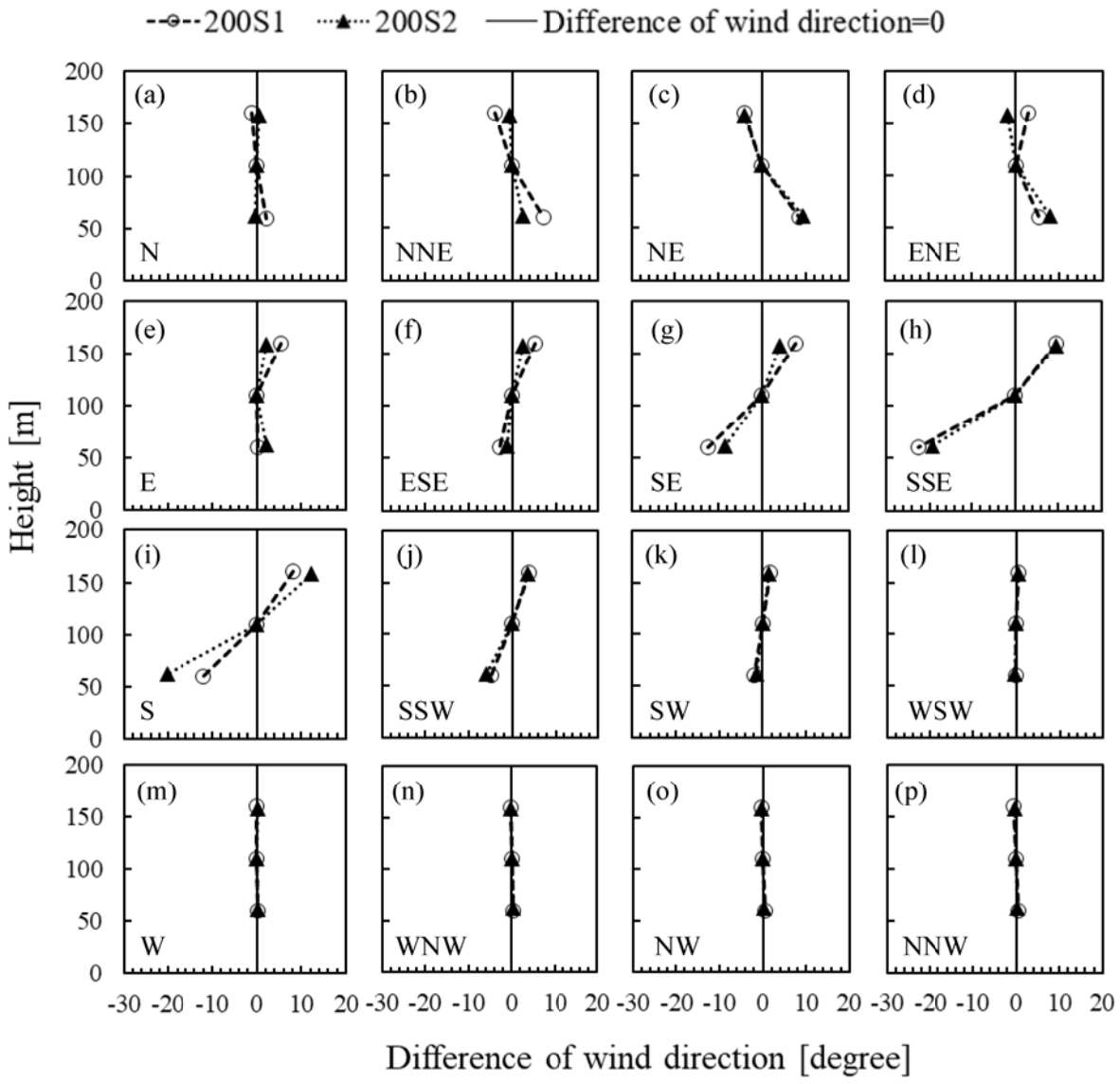

Figure 9. Vertical profile of wind direction

Figure 10 shows the horizontal distribution of normalized wind speeds in the east (E) and west (W) directions observed by 200S1 and 200S2. These wind directions are nearly perpendicular to the coastline and capture the effects of topography most clearly. As mentioned in section 2.2, 200S1 and 200S2 have contrasting landward topographies of high hills and a flat urban area, respectively. In the west direction, the wind speeds measured by 200S1 and 200S2 are greater offshore than those at points near land, while in the east (E) direction, the wind speed of land winds by 200S1 is less offshore than that at points close to land. During easterly winds, the wind speed measured by 200S1 at 3399 m offshore is 3.2% lower than the wind speed at 1179 m closer to land. This is because there is a mountain with an altitude of more than 100 m on the land side of 200S1 as shown in Figure 10 (a), and as the land wind moves offshore, the cross-sectional area increases, and the wind speed gradually decreases. Such speed reduction is not seen from 200S2 as shown in Figure 10 (b). This reflects the fact that the topography on the land side of 200S2 is low and the change in cross-sectional area is small. In general, wind speeds tend to be higher offshore, but because the cross-sectional area changes in coastal regions where mountains are nearby, wind speeds can be lower offshore.

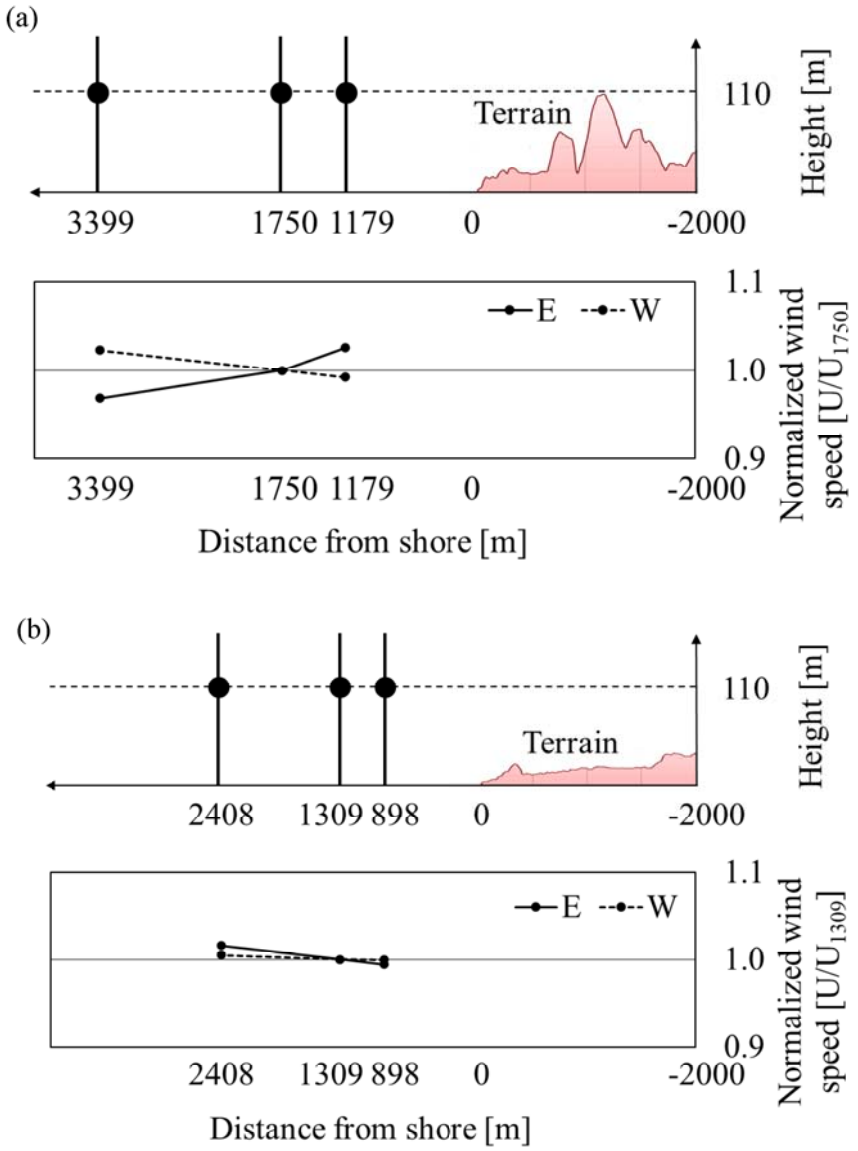

Figure 10. Horizontal distribution of mean wind speeds at 110 m height in the wind directions of E and W measured by (a) 200S1 and (b) 200S2

4. Conclusions

In this study, the effects of measurement range and precipitation on data availability of the scanning lidar measurements are investigated. The criteria of data filtering are proposed and validated by comparing the wind speeds and directions obtained by a single scanning lidar with those obtained by a met mast. Offshore wind measurements are carried out in two coastal regions using two single scanning lidars and used to determine the effect of onshore topography on the offshore wind. The conclusions of this study are summarized as follows.

(1) Since heavy rainfall and snowfall have a significant impact on data availability, a measurable range of 2 km or less is proposed for WindCube 200S scanning lidar measurements with high data availability.

(2) For single scanning lidar measurements, a minimum sector size of 39 degrees and a minimum data acquisition rate of 10% are proposed. The key performance indicators of the measured mean wind and direction based on the proposed criteria meet the requirements of best practice defined by the Carbon Trust.

(3) Results from one year of offshore wind measurements using single scanning lidars show that system availability and post-processed data availability meet the Stage 3 requirements proposed by the Carbon Trust.
(4) The vertical profiles of offshore wind speed in different wind directions are influenced by the stability of atmosphere. The horizontal distributions of offshore wind speed are affected by land topography. In coastal areas where mountains are nearby, wind speeds near the coast are higher than offshore wind speeds due to changes in vertical cross-sectional area.

References

[1] Yamaguchi A, Ishihara T 2016 A new motion compensation algorithm of floating Lidar system for the assessment of turbulence intensity *Journal of Physics, Conference Series* 753(7), pp.1-8
[2] Uchiyama S, Ohsawa T, Asou H, et al. 2022 Investigation on accuracy characteristics of floating LiDAR systems at the Mutsu Ogawara observation site. *Proc. of 44th Wind Energy Symposium,* 44, pp. 120-123 (in Japanese)
[3] Asakura T, Osawa T, Asou H 2022 Onshore oscillation experiment for verification of accuracy of wind observation by floating LiDAR system II *Proc. of 44th Wind Energy Symposium* 44, pp. 116-119 (in Japanese)
[4] Yamaguchi A, Kyomasu A, Ishihara T 2022 Turbulence measurement by using Doppler Lidar and its verification by using synthetic turbulent *Proc. of 44th Wind Energy Symposium* 44, pp. 160-163 (in Japanese)
[5] Watanabe K, Takakuwa S, Hemmi C, and Ishihara T 2021 A study of offshore wind assessment using dual-Doppler scanning Lidars *Journal of Wind Energy, JWEA* 45(2), pp.40-48 (in Japanese)
[6] Mano A, Ueno A, Itozaki S, Ishihara T 2021 Offshore wind assessment using single and dual scanning lidars, *Proc. of 43rd Wind Energy Symposium,* 43, pp. 164-167 (in Japanese)
[7] Shimada S, Goit J P, Ohsawa T, Kogaki T, Nakamura S 2020 Coastal wind measurements using a single scanning LiDAR. Remote Sensing 12: 1347
[8] Cheynet E, et al. 2021 The COTUR project: remote sensing of offshore turbulence for wind energy application. *Atmospheric Measurement Techniques* 14(9), pp. 6137-6157
[9] Cheynet E, et al. 2017 Measurements of surface-layer turbulence in a wide Norwegian fjord using synchronized long-range Doppler wind LiDARs. Remote Sensing 9(10): 977
[10] Goit J P, Yamaguchi A and Ishihara T 2020 Measurement and prediction of wind fields at an offshore site by scanning Doppler LiDAR and WRF, *Atmosphere*, 11, 442, pp.1-20
[11] Stephenson M, Clerc A 2016 Scanning LiDAR in offshore wind field testing scanning LiDAR systems in Dublin Bay. *Wind Europe Summit,* https://windeurope.org/summit2016/conference/allfiles/204_WindEurope2016presentation.pptx
[12] Simon E and Courtney M 2016 A Comparison of sector-scan and dual Doppler wind measurements at Høvsøre Test Station – one Lidar or two? *DTU Wind Energy*, Report E-0112
[13] NEDO 2023 Offshore wind measurement guidebook, *New Energy and Industrial Technology Development Organization,* https://www.nedo.go.jp/content/100962731.pdf
[14] The Carbon Trust 2018 OWA roadmap for the commercial acceptance of floating LiDAR technology, Version 2.0
[15] Ishihara T, Hibi K 2002 Numerical study of turbulent wake flow behind a three-dimensional steep hill, Wind and Structures, 5(2-4), pp.317-328
[16] Mano A, Ueno A, Itozaki S and Ishihara T 2023 A study of data availability and measurement accuracy of single scanning LiDAR for offshore wind assessment, *Journal of Wind Energy, JWEA*, 47(2), pp.44-54 (in Japanese)
[17] Ishihara T 2010 Guidelines for design of wind turbine support structure and foundations, Japanese Society of Civil Engineers, ISBN 978-4-8106-0705-5 (in Japanese)